catalysts

MDPI

Article

Understanding the Performance and Stability of Supported Ni-Co-Based Catalysts in Phenol HDO

Thuan M. Huynh [1,*], Udo Armbruster [2], Carsten R. Kreyenschulte [2], Luong H. Nguyen [1], Binh M. Q. Phan [1], Duc A. Nguyen [1] and Andreas Martin [2,*]

[1] Vietnam Petroleum Institute, 167 Trung Kinh, Cau Giay, 10000 Hanoi, Vietnam; luongnh.pvpro@vpi.pvn.vn (L.H.N.); binhpmq@vpi.pvn.vn (B.M.Q.P.); duc.a.nguyen@vpi.pvn.vn (D.A.N.)

[2] Leibniz-Institut für Katalyse e.V., Albert-Einstein-Str. 29a, 18059 Rostock, Germany; udo.armbruster@catalysis.de (U.A.); carsten.kreyenschulte@catalysis.de (C.R.K.)

* Correspondence: thuanhm.pvpro@vpi.pvn.vn (T.M.H.); andreas.martin@catalysis.de (A.M.); Tel.: +84-983-99-0010 (T.M.H.); +49-381-1281-246 (A.M.)

Academic Editor: Keith Hohn

Received: 11 October 2016; Accepted: 8 November 2016; Published: 11 November 2016

Abstract: Performances of bimetallic catalysts (Ni-Co) supported on different acidic carriers (HZSM-5, HBeta, HY, ZrO_2) and corresponding monometallic Ni catalysts in aqueous phase hydrodeoxygenation of phenol were compared in batch and continuous flow modes. The results revealed that the support acidity plays an important role in deoxygenation as it mainly controls the oxygen-removing steps in the reaction network. At the same time, sufficient hydrothermal stability of a solid catalyst is essential. Batch experiments revealed 10Ni10Co/HZSM-5 to be the best-performing catalyst in terms of conversion and cyclohexane yield. Complementary continuous runs provided more insights into the relationship between catalyst structure, efficiency and stability. After 24 h on-stream, the catalyst still reveals 100% conversion and a slight loss (from 100% to 90%) in liquid hydrocarbon selectivity. The observed alloy of Co with Ni increased dispersion and stability of Ni-active sites, and combination with HZSM-5 resulted in a well-balanced ratio of metal and acid sites which promoted all necessary steps in preferred pathways. This was proved by studies of fresh and spent catalysts using various characterization techniques (N_2 physisorption, X-ray diffraction (XRD), X-ray photoelectron spectroscopy (XPS), transmission electron microscopy (TEM) and infrared spectroscopy of adsorbed pyridine (pyr-IR)).

Keywords: Ni-Co alloy; bimetallic catalyst; phenol; aqueous phase hydrodeoxygenation; batch experiments; continuous flow reactor

1. Introduction

The major part of the presently consumed global energy is dependent on fossil fuels including oil, coal and natural gas. According to a British Petroleum p.l.c. statistical review of world energy, 86% of the energy consumed worldwide in 2014 comes from these sources [1]. To reduce the dependence on fossil fuel, also considering environmental concerns, renewable and sustainable energy is needed [2,3]. With its availability, renewability and CO_2 neutrality, biomass appears to be an alternative and sustainable resource for transportation fuels. The use of first-generation biofuels such as bioethanol and biodiesel (FAME—Fatty Acid Methyl Ester) has been established around the world for blending of conventional gasoline or diesel fuel. However, the use of edible oils and arable land for biofuels competes with the food supply chain and affects availability and prices. Nevertheless, the governments of many countries set ambitious goals to promote the use of renewable sources, e.g., the U.S. Department of Energy has set a target to produce 20% of transportation fuel from biomass [4].

Several technologies for production of second-generation fuels (utilizing complete biomass) like gasification (and subsequent Fischer-Tropsch process), hydrothermal upgrading and pyrolysis

are developing. Bio-oil, e.g., obtained from fast pyrolysis of biomass, is considered a promising feedstock for liquid fuel production; however, its quality is far away from conventional fuels due to its high water and oxygenates content. This necessitates additional treatment to remove oxygen in general. Among available technologies, hydrodeoxygenation (HDO), which is performed at high pressure of external hydrogen (50–300 bar) at moderate and high temperature (200–450 °C) in the presence of a heterogeneous catalyst, has evolved quickly into a major technology for bio-oil upgrading. The commercial NExBTL (Neste Oil) leading to HVO (hydrogenated vegetable oil) and the similar Ecofining (UOP/Eni) processes are two prime HDO examples.

Nonetheless, analysis of bio-oil and evaluation of conversion processes are still challenging due to the complex mixture with a high number of functionalities. As a result, particularly at bench scale, more attention has been put on studies of individual model compounds to get more insight into the chemistry before switching to bio-oil. Therefore, the rather less reactive phenolic compounds (phenol, catechol, anisole, guaiacol) have attracted significantly more attention compared to other groups like furanes, acids, aldehydes, ketones and alcohols [5,6].

To take advantage of available hydroprocessing technology of the conventional refinery, the same catalysts and conditions were applied for bio-oil HDO in the first known studies. However, the hydrodesulfurization (HDS) catalysts (sulfides of CoMo or NiMo/γ-Al_2O_3) deactivated quickly due to loss of sulfur and coke deposition and the support is unstable against the abundant amount of water in bio-oil [7,8]. Meanwhile, commercial hydrotreatment catalysts (e.g., supported noble metal catalysts with Pt, Pd, Ru, Rh) show much higher activity and stability than HDS catalysts [9–20]. However, such precious metal catalysts are much more expensive than HDS catalysts, thus further progress is needed to realize viable economic alternative formulations.

Various supported non-noble monometallic catalysts (such as Fe/SiO_2, Co/SiO_2, copper chromite, and Ni-based catalysts) have been already used in HDO studies [21–26]. Although Ni-based catalysts showed the highest activity, coke deposition and deactivation due to Ni agglomeration and leaching into aqueous phase are still a problem [21,23]. Few groups also reported on bimetallic catalysts for HDO of model compounds and bio-oil due to their properties being different compared to the corresponding monometallic catalysts [27]. It was reported that bimetallic Ni-Cu/δ-Al_2O_3 catalysts improve product properties of HDO oil [28]. Bimetallic Ni-Pt/γ-Al_2O_3 and Co-Pt/γ-Al_2O_3 catalysts show high conversion and change the product selectivity in HDO of m-cresol compared to monometallic Pt/γ-Al_2O_3 catalysts [29]. Other groups reported on the HDO of model compounds (e.g., m-cresol, guaiacol) or bio-oil over bimetallic catalysts such as Pt-Fe/C, Ni-Fe/SiO_2, Ni-Fe/Al_2O_3 [30–34]. For instance, vapor phase HDO of guaiacol using Pd-Fe/C catalyst significantly improved HDO yield for toluene/benzene/trimethylbenzene (80%) compared to Fe/C and Pd/C monometallic catalysts [30]. Besides the fact that the precious metal catalysts rule out the application, the hydrothermal stability of some supports (e.g., Al_2O_3) was limited. More insights into the HDO of model compounds and bio-oil have been given in relevant reviews [35–38].

As stated above, phenols are refractory at the desired reaction conditions and therefore suited as probe compounds to understand the fundamental chemistry of HDO reaction. Depending on types of catalysts and reaction conditions (temperature, pressure, solvent properties, etc.), there are two main reaction pathways to eliminate oxygen from phenol, either the direct deoxygenation to benzene (DDO route) or the hydrogenation of the aromatic ring followed by dehydration for oxygen removal (HYD route) [10,21,39]. This suggests that multiple chemical transformations are needed which require different sites to activate hydrogen and to cleave C–O bonds. Depending on the catalyst nature, several possible active sites for phenol HDO reaction have been proposed. In bifunctional catalysts, metal sites and acid sites (e.g., oxides of oxophilic metals like MoO_3, Al_2O_3, WO_3, ZrO_2 or zeolites) are present at the same time and are involved in the steps along the reaction pathways [8,22,39,40]. In extension, few kinetic studies on HDO of phenol on different catalysts, e.g., Co-MoS_2/Al_2O_3 [39], Pd/C, Ru/C, Rh/C or Ni catalysts combined with several aqueous acidic solutions (e.g., H_3PO_4, CH_3COOH and Nafion® solution), or solid acids (HZSM-5, Nafion®/SiO_2, ZrO_2) are known [19,22,23]. Rate-determining steps

in the reaction sequence for phenol HDO strongly depend on the nature of catalyst (metal and acid sites) and reaction conditions.

Most of the mentioned model studies were carried out either in batch autoclaves with short run times [16,19–23,41] or under gas phase reaction conditions [30–33,42]. Recent HDO studies reported application of continuous flow reactors using organic solvents (e.g., 1-octanol, 1-octane, 1-hexane) [43–45] or supercritical water [46]. Those studies often have not put the focus on the spent catalysts after long-term reaction. However, understanding of catalyst structure and stability is crucial for development of an effective catalyst. Compared to a batch reactor, the use of a continuous reactor is favorable because it allows long-term studies to not be limited by chemical equilibrium. In addition, it provides better kinetic control of reaction steps which helps to elucidate complex reaction networks. The mechanisms are different in gas phase and aqueous phase reactions due to solvent effects, different concentration profiles on the catalyst surface and mass transfer limitations [47]. From a technological point of view, continuous and heterogeneously catalyzed operation is often preferred, e.g., as catalyst separation from products is no issue.

In recent batch studies, we have developed supported bimetallic Ni-Co catalysts (homogeneous Ni-Co alloy), which were successfully tested in aqueous phase HDO of phenol, to replace noble metal catalysts and to overcome known drawbacks (deactivation, coke formation, costs) [48,49]. Batch runs (250 °C, 2 h) revealed that bimetallic catalysts with an equimolar Ni:Co ratio (10 wt % each on HZSM-5) outperformed monometallic Co, Cu and Ni, bimetallic Ni-Cu and Ni-Co catalysts with other metal ratio in terms of conversion and yield toward saturated hydrocarbons. Moreover, the bimetallic Ni-Co catalysts formed significantly less coke deposits. However, similar to previous studies, these short-time batch tests did not give satisfactory information about catalyst stability.

Thus, various bimetallic Ni-Co catalysts with different acidic supports and a corresponding monometallic catalyst as a benchmark were tested in both a batch autoclave and a continuous fixed bed reactor setup. Long-term experiments together with characterization of fresh and spent catalysts using various techniques (N_2 physisorption, XRD, XPS, TEM, IR) indicated crucial features and gave more insight into reaction network and catalyst stability.

2. Results and Discussion

2.1. Characterization of Fresh and Pre-Reduced Catalysts

Table 1 summarizes selected properties of fresh and pre-reduced monometallic Ni and bimetallic Ni-Co catalysts supported on HZSM-5, which stem from our previous studies on their performance in HDO of phenol in batch mode [48,50]. The catalysts are denoted as *x*Ni*y*Co/Z, where *x* and *y* are the rounded content (wt %) of nickel and cobalt, respectively, and Z is the support.

Table 1. Textural and acidic properties of fresh and pre-reduced catalysts.

Catalysts	V_{N2} (Adsorbed at STP) [1]	S_{BET}	S_{micro} [2]	V_t [3]	V_{micro} [4]	Metal Crystallite Size [5]	Acidity		
							BS [6]	LS [7]	BS:LS
	(cm^3/g)	(m^2/g)	(m^2/g)	(cm^3/g)	(cm^3/g)	(nm)	(μmol/g)		
10Ni10Co/ZrO_2	12.1	40	-	0.16	-	29.8	0	44	-
10Ni10Co/HBeta	101.5	434	368	0.24	0.16	23.3	137	984	0.14
10Ni10Co/HY	131.8	568	499	0.32	0.20	19.0	259	505	0.51
10Ni10Co/HZSM-5	65.4	281	195	0.23	0.09	15.1	162	509	0.32
21Ni/HZSM-5	65.4	281	184	0.25	0.08	29.7	243	345	0.70

[1] STP: Standard temperature and pressure (1 bar, 0 °C); [2] S_{micro} = micropore area; [3] V_t = total pore volume; [4] V_{micro} = micropore volume; [5] calculated from X-ray diffraction (XRD) data; [6] BS = Brønsted acid sites; [7] LS = Lewis acid sites.

The surface areas (S_{BET}) determined using fresh catalyst samples, as calculated from the adsorbed N_2 volume, follow the support order: HY > HBeta > HZSM-5 > ZrO_2. Fresh and pre-reduced samples show very similar S_{BET} as the comparison of S_{BET} data from one such couple showed. The sample

10Ni10Co/ZrO_2 (with a non-acidic support) had a mesoporous structure and its S_{BET} was significantly lower compared to the other catalysts. The average metal particles' crystallite size (calculated from XRD results by Scherrer's equation) revealed that 10Ni10Co/HZSM-5 presents the smallest crystallites with 15 nm, whereas in the other catalysts they varied from 19–30 nm. It is remarkable that the crystallites in 10Ni10Co/ZrO_2 at the same metal loading are of similar size, even though the surface area is the lowest and a lower dispersion is expected. The XRD patterns of the pre-reduced catalysts are displayed and discussed below together with the results for the spent samples.

The amounts of Brønsted (BS) and Lewis (LS) acid sites of pre-reduced catalysts were calculated from integral intensities of the peaks at 1543 and 1450 cm^{-1} in the infrared spectra of adsorbed pyridine (pyr-IR) [51] shown below and the molar extinction coefficient [52]. The BS concentrations follow the support order: HY > HZSM-5 > HBeta > ZrO_2 (see Table 1). After normalizing to the specific surface area, the respective BS portions show another trend: HZSM-5 > HY > HBeta > ZrO_2, pointing to the high acidity of HZSM-5 support. As the density of Lewis acid sites in 10Ni10Co/HBeta is much higher than for other samples, 10Ni10Co/HBeta has the highest total acidity within this series.

2.2. Effect of Support Nature on Bimetallic Ni-Co Catalyst Performance

Batch runs in aqueous phase HDO of phenol using catalyst in powder form were conducted to study the support impact (5.3 mmol of phenol, 10 g of H_2O, 25 mg of catalyst, 250 °C, 50 bar H_2 at room temperature (RT)) in our preceding study [48] revealing that supported Ni and Ni-Co catalysts lead to deoxygenated products (cyclohexane, benzene, cyclohexene, methylcyclopentane (MCP)) and oxygenated products (cyclohexanol, cyclohexanone) under given conditions. The bimetallic catalyst 10Ni10Co/ZrO_2 allowed complete conversion within only 60 min but hydrocarbon selectivity was less than 12%. It appears that the latter was limited by the poor acidity of ZrO_2 compared to the zeolites and rather big metal particles (see Table 1). It is well known that metal particle size reveals a significant influence on catalytic performance. Mortensen et al. very recently showed the impact of Ni particle size of rather non-acidic Ni/SiO_2 catalysts on HDO of a phenol model compound [53]. Deoxygenation rate increases with decreasing particle size, while phenol conversion simultaneously drops. Regardless, HY- and HBeta-supported catalysts showed much higher selectivity toward deoxygenated products. However, HZSM-5-based solids were clearly the most active, and conversion reached nearly 100% after 60 min. The selectivity to hydrocarbons on 10Ni10Co/HZSM-5 was 90% and slightly higher compared to a monometallic catalyst, thus making it the best-performing catalyst. This was attributed to the metal particle dispersion, support acidity and hydrothermal stability [48]. However, the value of these runs was somehow limited as intermediate sampling was not possible, and thus the true deactivation behavior was not disclosed.

In the present study, the same catalysts, albeit shaped as pellets (180–250 µm), were tested in a continuous flow reactor at similar conditions (250 °C, 60 bar, weight hourly space velocity (WHSV) = 1.8 h^{-1}, 3 wt % phenol in H_2O, H_2:phenol molar ratio = 28). The blank test without catalyst showed that already 8% conversion was obtained due to the impact of hot compressed water and wall effects. It is known that hot compressed water is different compared to ambient water (e.g., lower pH, lower dielectric constant, fewer and weaker hydrogen bonds) and might act as a reactant [54,55]. The conversion and product distribution of the catalyst test runs as a function of time-on-stream (TOS) are presented in Figure 1.

All catalysts show complete conversion over entire TOS except 10Ni10Co/HY, which reached a maximum conversion of 90% after 2 h, but deactivated at progressive TOS. This might be due to its low hydrothermal stability and acidity loss (see Table 2 and XRD pattern below in Figure 2 in Section 2.3). Significant differences in selectivity to products were observed for the named catalysts. With the least acidic 10Ni10Co/ZrO_2, mainly cyclohexanol formed with more than 95% selectivity, whereas highly acidic 10Ni10Co/HZSM-5 and 10Ni10Co/HBeta led to nearly 100% selectivity to hydrocarbon products during the first 6 h on-stream. However, with progressive TOS, a slight rise of cyclohexene and benzene fraction with 10Ni10Co/HZSM-5 and of cyclohexanol in case of 10Ni10Co/HBeta at the

expense of cyclohexane selectivity was obtained. These observations point to a slight deactivation of the metal sites for H_2 activation as well as of acidic sites. With the monometallic catalyst 21Ni/HZSM-5, the selectivity to benzene and cyclohexene was always higher than with 10Ni10Co/HZSM-5. This is in line with the results from the previous batch tests and confirms the outstanding capability of Ni-Co alloy in individual hydrogenation steps.

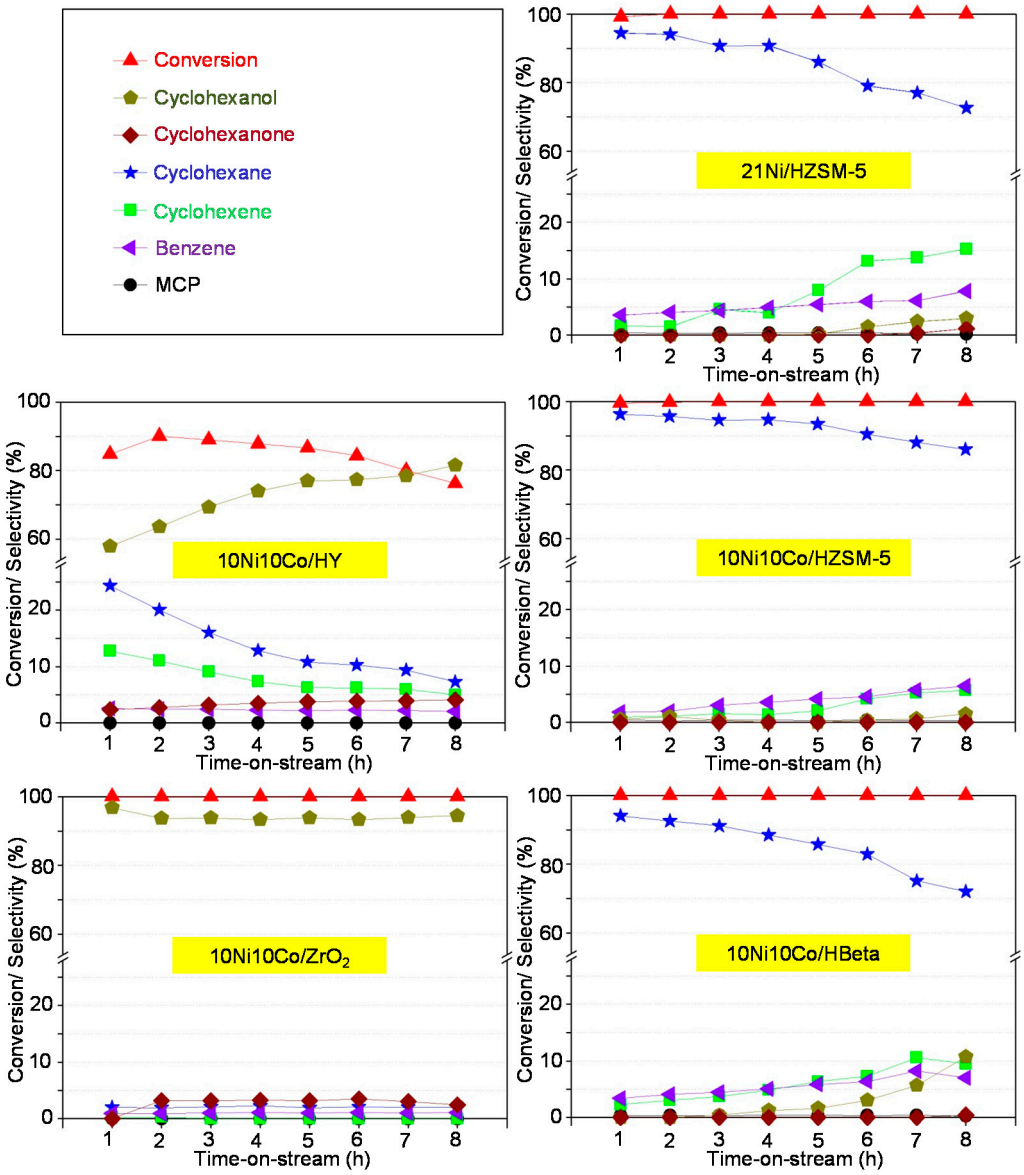

Figure 1. Phenol hydrodeoxygenation (HDO) over various catalysts in the continuous reactor (T = 250 °C, 60 bar H_2, weight hourly space velocity (WHSV) = 1.8 h^{-1}, 3 wt % phenol in H_2O, H_2: phenol molar ratio = 28).

Table 2. Textural and acidic properties of the spent catalysts.

Catalysts	V_{N2} (Adsorbed at STP) [1]	S_{BET}	S_{micro} [2]	V_t [3]	V_{micro} [4]	Metal Crystallite Size [5]	Coke	Acidity		
								BS [6]	LS [7]	BS:LS
	(cm^3/g)	(m^2/g)	(m^2/g)	(cm^3/g)	(cm^3/g)	(nm)	(wt %)	(μmol/g)		
10Ni10Co/ZrO_2 [8]	12.4	44	-	0.17	-	29.6	0.6	15	41	0.37
10Ni10Co/HBeta [8]	27.4	117	98	0.20	0.04	30.7	1.7	50	189	0.27
10Ni10Co/HY [8]	16.4	71	45	0.19	0.02	35.3	0.7	29	125	0.23
10Ni10Co/HZSM-5 [8]	62.3	265	190	0.30	0.08	22.2	1.0	112	440	0.25
21Ni/HZSM-5 [8]	63.8	271	198	0.29	0.08	31.7	1.9	117	251	0.47
10Ni10Co/HZSM-5 [9]	41.2	176	143	0.22	0.06	31.1	1.3	91	434	0.21
21Ni/HZSM-5 [9]	33.4	142	136	0.14	0.06	38.4	3.9	129	188	0.68

[1] STP: Standard temperature and pressure (1 bar, 0 °C); [2] S_{micro} = micropore area; [3] V_t = total pore volume; [4] V_{micro} = micropore volume; [5] calculated from XRD data; [6] BS = Brønsted acid sites; [7] LS = Lewis acid sites; [8] 8 h on-stream, T = 250 °C, p = 60 bar, WHSV = 1.8 h^{-1}, H_2:phenol molar ratio = 28; [9] 24 h on-stream, T = 250 °C, p = 60 bar, WHSV = 1.8 h^{-1}, H_2:phenol molar ratio = 28.

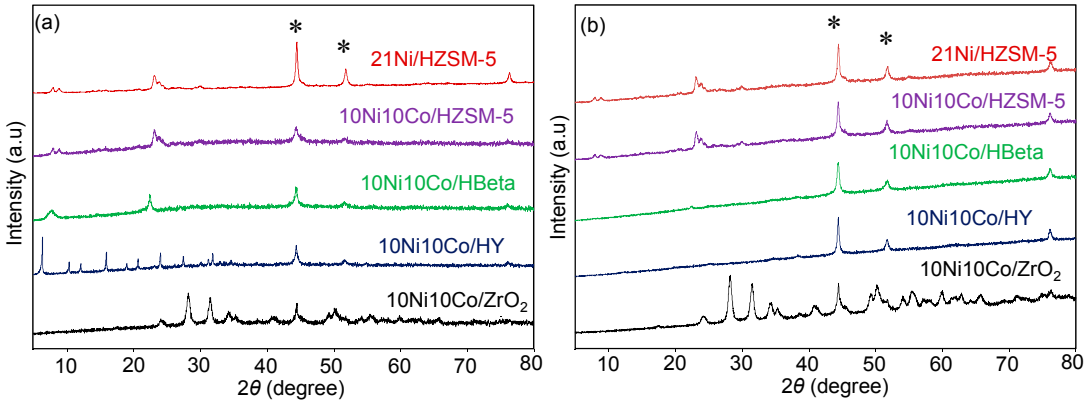

Figure 2. X-ray powder diffraction (XRD) patterns of pre-reduced (**a**) and spent catalysts (**b**) from HDO runs in the continuous reactor (T = 250 °C, p = 60 bar H_2, WHSV = 1.8 h^{-1}, 3 wt % phenol in H_2O, H_2:phenol molar ratio = 28, 8 h on-stream; * 2θ = 44.4° and 51.7° (powder diffraction file (PDF) for Ni-Co [01-074-5694]).

The continuous runs clearly proved the impact of supports on the reaction network, the individual reaction steps and finally on the selectivity, thereby providing better insight into consecutive reactions. The better control of residence time compared to batch runs affected the reaction rates, and deoxygenation was more effective. In particular, cyclohexanol formation decreased and selectivity to cyclohexane increased (e.g., using 10Ni10Co/HBeta).

As discussed above, the observed catalytic activity does not match consistently with individual factors like acid strength as listed above in Table 1. Compared to 10Ni10Co/ZrO_2, the zeolite-supported samples have higher acidity and thus show higher selectivity to deoxygenated products for both batch and continuous reactors. Additionally, the hydrothermal stability is an important feature when discussing the catalytic results. The 10Ni10Co/HZSM-5 showed higher activity and deoxygenation selectivity compared to 10Ni10Co/HY and 10Ni10Co/HBeta, as the crystalline framework character of HY and HBeta deteriorated during the reaction (see Section 2.3).

On the other hand, Ni-Co alloy again proved to reach superior hydrogenation impact as compared to monometallic Ni reference [48,49]. This confirms nicely the results from the batch HDO studies. Consequently, 10Ni10Co/HZSM-5 was further evaluated in continuous mode at different temperatures, pressures and contact times and in a prolonged test to understand the catalyst stability (Section 2.4).

2.3. Spent Catalyst Characterization Results

The spent supported 10Ni10Co catalysts were recovered from the continuous flow reactor after 8 h TOS, characterized and compared with the pre-reduced ones. The XRD patterns of the two groups of catalysts are shown in Figure 2. The main reflections of the Ni-Co catalysts appear at 2θ = 44.4° and 51.7° (powder diffraction file (PDF) for Ni-Co [01-074-5694]) pointing to the existence of Ni-Co alloy metal particles because these positions are in between those of the pure metals (cf. PDF for Ni [01-077-8341] and PDF for Co [01-077-7456]). The existence of Ni-Co alloys is also proven by TEM as shown below. The patterns of spent catalysts represent the same structural features as observed for the spent samples from batch runs [48]. The sharp support reflections in 10Ni10Co/HY in the range of 6°–32° almost disappeared after 8 h on-stream, indicating the transformation of the crystalline framework structure of zeolite Y into an amorphous phase [56]. Similarly, XRD patterns indicated a significant decrease in intensity of the zeolite Beta reflections (2θ = 4.5°, 23°). In contrast, ZrO_2 and HZSM-5-supported catalysts showed no appreciable change in support reflections.

Besides an alteration of the crystallinity of some supports, the crystallite size of Ni particles in pure Ni-containing catalysts and Ni-Co alloy particles in Ni-Co solids seems to be increased for all zeolite-supported catalysts as listed in Table 2. The data point to particle growth which may decrease the hydrogenation activity due to lower dispersion. Therefore, the hydrogenation depth might deteriorate with TOS. Table 2 also lists the textural and acid properties of the spent catalysts. The S_{BET} of spent 10Ni10Co/HY and 10Ni10Co/HBeta dropped significantly compared to those of fresh catalysts (compare entries 2 and 3 in Tables 1 and 2), providing further proof of the vast destruction of these support structures, in accordance with XRD data. Interestingly, the decays in the S_{BET} of spent ZrO_2 and HZSM-5-supported catalysts (entries 1 and 4) were negligible (6%, 4%). Nonetheless, after 24 h on-stream (entries 6 and 7), the S_{BET} of spent 10Ni10Co/HZSM-5 dropped by 37%, whereas 21Ni/HZSM-5 lost 49%. These losses may also have slightly contributed to catalyst deactivation as discussed below. The stronger decline in S_{BET} of spent 21Ni/HZSM-5 was possibly also related to the higher amount of coke deposits as shown in Table 2, being 3 times higher than for 10Ni10Co/HZSM-5.

Weakly acidic 10Ni10Co/ZrO_2 showed a slight increase in the number of BS, probably by hydration of the surface due to hydrothermal reaction conditions, whereas the total acidities of 10Ni10Co/HY and 10Ni10Co/HBeta decreased drastically by 80 and 79%, respectively (compare entries 1–3 in Tables 1 and 2). Figure 3 depicts 10Ni10Co/HZSM-5 pyr-IR spectra; the total acidity decreased moderately after 8 h on-stream by 18% (entry 4 in Table 2). Spectra for 21Ni/HZSM-5 (entry 5 in Tables 1 and 2) reveal a loss of acid sites (37%), and simultaneously strong Lewis sites (1450, 1622 cm^{-1}) were transformed into weaker ones (1444, 1597 cm^{-1}). This might be attributed to the loss of protonated oxide bridges during reaction in aqueous environment [57]. When running the HZSM-5-supported catalysts in separate runs over 24 h, deactivation proceeded, but slower than within the first 8 h (entries 6 and 7 in Table 2).

Table 3 presents the changes in elemental composition of the near-surface region of the HZSM-5-supported catalysts as measured by XPS. The Ni:Si ratio in 21Ni/HZSM-5 for all three samples was nearly constant, whereas for 10Ni10Co/HZMS-5 an increase of Ni and Co near-surface concentrations was observed comparing the fresh pre-reduced and the spent catalysts.

These spent samples of 10Ni10Co/HZSM-5 and 21Ni/HZSM-5 were also studied by TEM. Similar to fresh 10Ni10Co/HZSM-5 (Figure 4a), the sample obtained after 8 h on-stream presents a broad size distribution of particles with different shapes (Figure 4b). Besides compact particles, some band-like metallic species (indicated by arrows) appeared. According to additional energy dispersive X-ray spectroscopy (EDXS) analyses, they consist of Ni-Co alloy located on the external surface of support HZSM-5. These observations are not fully understood, but may be due to agglomeration and re-structuring of metal sites during reaction. It should be noted that metal particles might recrystallize under TEM measurement conditions due to collapse of support HZSM-5 structure by harsh electron

bombardment [48]. However, the Ni:Co atom ratio was in the same range as for the pre-reduced catalyst (41:59–59:41).

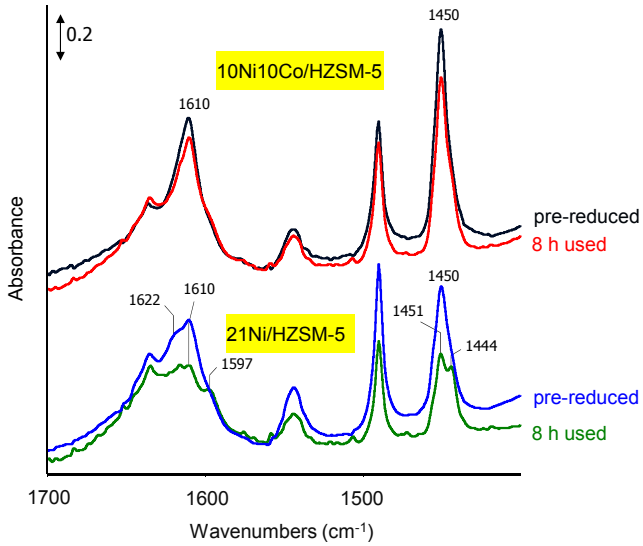

Figure 3. Infrared spectra of adsorbed pyridine (pyr-IR spectra) of pre-reduced and spent HZSM-5-supported catalysts (after 8 h on-stream).

Table 3. Elemental composition of the near-surface region of fresh pre-reduced and spent catalysts.

Samples	21Ni/HZSM-5	10Ni10Co/HZSM-5	
	Ni:Si Ratio	Ni:Si Ratio	Co:Si Ratio
Pre-reduced	0.11	0.04	0.06
8 h used	0.10	0.09	0.13
24 h used	0.12	0.09	0.14

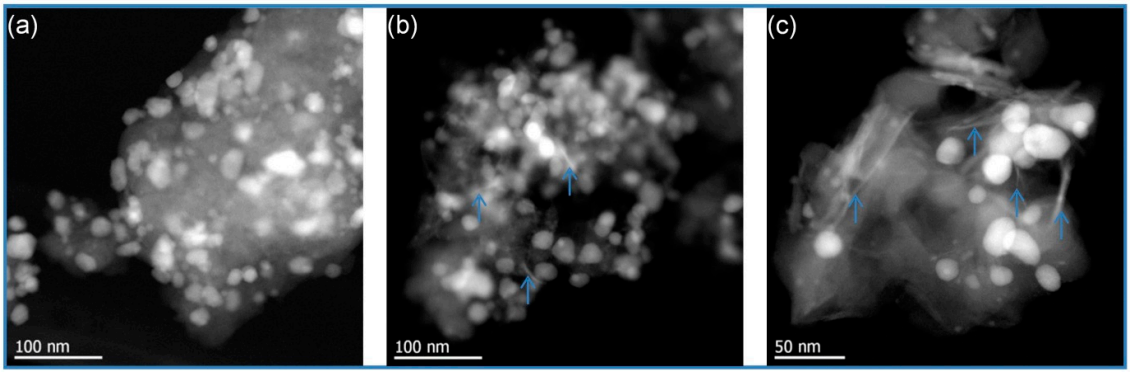

Figure 4. Transmission electron microscopy (TEM) images of 10Ni10Co/HZSM-5: (**a**) pre-reduced; (**b**) after 8 h on-stream and (**c**) after 24 h on-stream (arrows indicate the band-like particles).

After 24 h on-stream, 10Ni10Co/HZSM-5 showed a broad size distribution of particles and the band-like particles were still observed (Figure 4c). The latter seem to get more pronounced with TOS. However, only a minor change in Ni:Co atom ratio, as found in a few particles (65:35), was noticed besides residual particles with the same composition as a fresh pre-reduced catalyst (41:59–59:41) after 24 h on-stream. Conversely, different types of crystallites were present in 21Ni/HZSM-5 after 8 h

on-stream; especially the band-like structures were much more pronounced (Figure 5a,b). In addition, very large Ni particles appeared. After 24 h on-stream, the 21Ni/HZSM-5 catalyst clearly showed strong Ni agglomeration resulting in large metal particles up to 110 nm (Figure 5c).

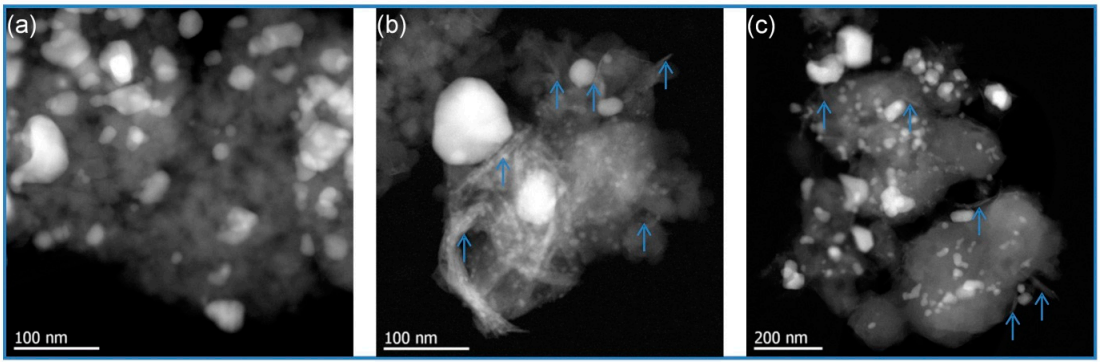

Figure 5. TEM images of 21Ni/HZSM-5. (**a**) Pre-reduced; (**b**) after 8 h on-stream and (**c**) after 24 h on-stream (arrows indicate the band particles).

Although both catalysts showed a change in metal particle sizes and the formation of band-like particles, the effect was much more pronounced in the case of 21Ni/HZSM-5 compared to 10Ni10Co/HZSM-5. This is also in line with the crystallite size derived from XRD (see Table 2). It can be concluded that the presence of Co slows down the crystal growth and stabilizes the Ni active sites during the long-term reaction owing to the formation of Ni-Co alloy.

All these observations (loss in S_{BET}, deactivation of acid and metal sites) explain why the monometallic catalyst deactivated much faster than the bimetallic catalyst.

2.4. Effect of Reaction Conditions

2.4.1. Effect of Pressure and Temperature

The impact of pressure and temperature on the performance of 10Ni10Co/HZSM-5 in the batch reactor is depicted in Figure 6a. At 200 °C and without limitation by H_2 shortage, only hydrogenation of phenol toward cyclohexanol proceeded at a remarkable rate, leading to nearly complete conversion. Raising the temperature to 225 °C caused an extreme drop in cyclohexanol selectivity and a complementary boost in cyclohexane formation. Obviously, this small temperature step was sufficient to provide the necessary activation energy for the dehydration of cyclohexanol, which is essential in HYD reaction route. With a further temperature increase, cyclohexane selectivity passed a maximum of 92% at around 250 °C; however, above this temperature, more and more benzene was formed instead. This is no surprise because the higher temperature promotes dehydration and dehydrogenation which are endothermic reactions [58]. The temperature dependence was cross-checked by additional batch experiments with cyclohexanol as starting material at an initial H_2 pressure of 50 bar. At 200 °C, conversion was less than 70%. At 250 °C, conversion and cyclohexane selectivity reached 99% and 97%, respectively. This result is also in line with the work of Zhao et al. who showed that cyclohexanol conversion in presence of aqueous H_3PO_4 significantly rose from 8.6% to 95% with increasing temperature from 180 to 200 °C [19]. In addition, the same group also showed that raising the temperature in HDO of 4-*n*-propylphenol over Pd/C combined with various solid acids (e.g., HZSM-5, Amberlyst 15, sulfated zirconia) leads to more oxygen-free products [41]. When repeating this test with bare support HZSM-5, cyclohexanol conversion was almost as high, but cyclohexene was formed instead of cyclohexane with 95% selectivity.

Consequently, another series of runs with 10Ni10Co/HZSM-5 was carried out at a temperature of 250 °C and various initial H_2 pressures (Figure 6b). Obviously, raising the pressure led to an increase of the selectivity to saturated hydrocarbons, i.e., cyclohexane. The increased H_2 solubility in the bulk

phase increases its concentration near the metal sites, finally boosting the H_2-consuming reactions (e.g., hydrogenation of phenol, benzene and cyclohexene). With a H_2 pressure of 20 bar at RT, the selectivity for oxygenated products (cyclohexanol, cyclohexanone) reached approximately 20% at 82% conversion within 1 h, whereas the cyclohexane selectivity did not exceed 40%. With a H_2-filling pressure of 60 bar, cyclohexane selectivity amounts to 94% at complete conversion.

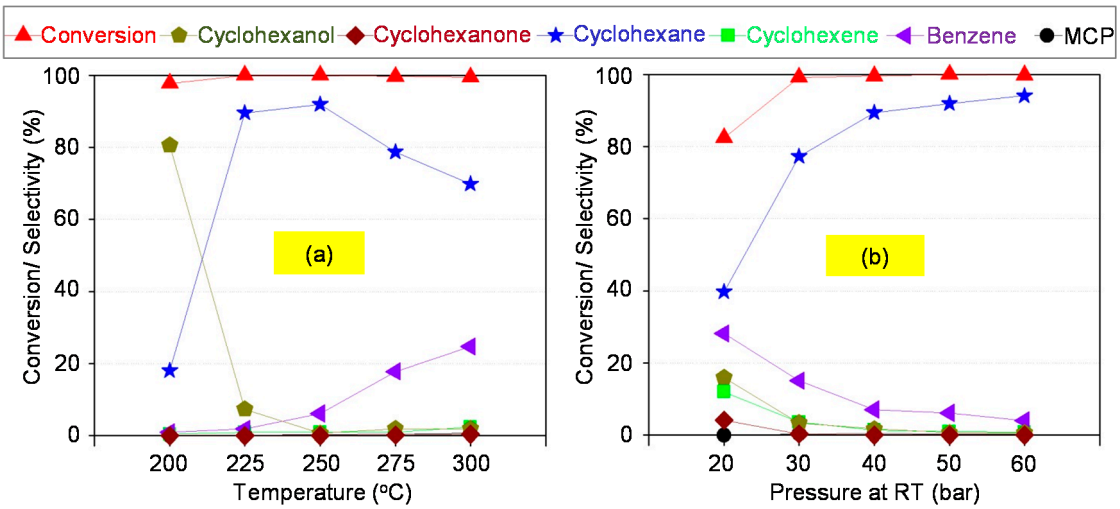

Figure 6. Effect of (**a**) temperature and (**b**) pressure on phenol HDO with 10Ni10Co/HZSM-5 in the batch reactor (5.3 mmol of phenol, 10 g of H_2O, 25 mg of catalyst, t = 1 h).

Complementary runs on phenol HDO in continuous mode were carried out at favored conditions (60 bar, WHSV = 1.8 h^{-1}). It is noteworthy that the hydrogen partial pressure was lower than in the batch runs (60 bar at RT) but constant, whereas in the batch runs the partial pressure decreased with ongoing reaction. Almost complete phenol conversion over 10Ni10Co/HZSM-5 was reached in the temperature range of 200–300 °C, whereas a slight drop in conversion was observed in the final set point at 350 °C (Figure 7). This might be due to some catalyst deactivation via structural changes or deposition of high-boiling components. At the same time, benzene, cyclohexene and MCP selectivities increased to 34%, 2% and 6%, respectively, at the expense of cyclohexane. This points to accelerated reaction rate of cyclohexane dehydrogenation to cyclohexene and benzene and control by chemical equilibrium. These unsaturated products could act as precursors for coke formation, which in turn limits catalyst lifetime. Simultaneously, MCP might form via isomerization of cyclohexane in the presence of BS. It is well known that isomerization and dehydrogenation are favored at high temperature and/or the presence of strong acid catalysts [59]. Similarly, Echeandia et al. reported that in phenol HDO the MCP selectivity rose from 0 to 17% when the temperature increased from 250 to 300 °C on Pd/HY catalyst [44]. Furthermore, cyclohexanone was detected at 350 °C (see Figure 7), indicating slower hydrogenation on metal sites, probably due to equilibrium control, because otherwise this intermediate was rapidly hydrogenated to cyclohexanol on metal sites [48]. As a result, 250 °C was selected as optimum temperature for further investigation on the HDO of phenol in continuous regime.

The effect of pressure on 10Ni10Co/HZSM-5 performance in continuous HDO of phenol was studied at given conditions (250 °C, 3 wt % phenol in H_2O, WHSV = 1.8 h^{-1}, H_2:phenol molar ratio = 28) from 40 to 100 bar (Table 4). For each test, a fresh sample was loaded into the reactor. The test at 40 bar exhibited high yields of oxygenates and unsaturated hydrocarbons in accordance with the batch tests. Raising the pressure to 100 bar significantly increased the cyclohexane selectivity from 78% to 99% after 1 h on-stream. A gradual drop in cyclohexane selectivity occurred with longer TOS (e.g., at 60 bar: from 96% to 95% after 4 h and to 86% after 8 h), together with a slight increase of cyclohexene, benzene and cyclohexanol selectivities. This points first to a deteriorated performance of the acid sites at high pressure. Second, the competitive adsorption

of phenol and intermediates onto metal and acid sites should be considered. Phenol and polar intermediates (cyclohexanol, cyclohexanone) might prefer acidic BS, whereas non-polar products (benzene, cyclohexene, cyclohexane, MCP) prefer metal sites. The degree of surface coverage is controlled in each case by adsorption/desorption equilibria which depend also on total pressure. H_2 is mostly adsorbed on metal sites, too, and therefore high H_2 pressure might hamper adsorption of intermediates. As a result, the pressure of 60 bar was selected for further investigation.

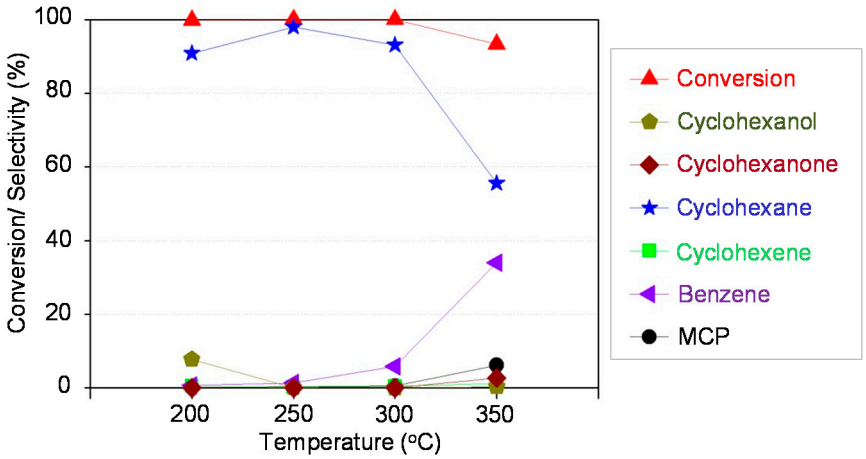

Figure 7. Temperature effect on phenol HDO over 10Ni10Co/HZSM-5 in continuous mode (250 °C, 60 bar, WHSV = 1.8 h^{-1}, H_2:phenol molar ratio = 28).

Table 4. Effect of pressure on the performance of 10Ni10Co/HZSM-5 in the continuous reactor.

TOS (h)	*p* (bar)	Conversion (%)	Selectivity (%)					
			Cyclo-hexane	Benzene	Cyclo-hexene	MCP	Cyclo-hexanol	Cyclo-hexanone
1	40	100	77.7	9.6	8.3	0.3	4.1	-
	60	99	96.3	1.8	0.9	0.5	0.5	-
	80	100	97.3	1.1	1.3	0.3	-	-
	100	100	99.1	0.6	-	0.3	-	-
4	40	100	71.6	8.6	11.2	0.3	7.6	0.8
	60	100	94.6	3.6	1.4	0.4	-	-
	80	100	95.2	1.4	3.1	0.3	-	-
	100	100	97.9	1.3	0.4	0.4	-	-
8	40	100	60.4	8.6	16.2	0.3	12.7	1.8
	60	100	86.0	6.5	5.7	0.3	1.5	-
	80	100	85.2	3.9	8.1	0.4	2.5	-
	100	100	85.7	1.7	5.0	0.3	7.2	-

Reaction conditions: T = 250 °C, WHSV = 1.8 h^{-1}, H_2:phenol molar ratio = 28.

2.4.2. Effect of Space Velocity (WHSV)

Table 5 compares the performance of 10Ni10Co/HZSM-5 at different WHSV from 1.8 to 3.0 h^{-1} at favored conditions (250 °C, 60 bar). Phenol conversion is complete after 8 h on-stream at any given WHSV; however, a clear change in selectivity is evident. After 1 h on-stream, the accumulated selectivity toward deoxygenated products reaches nearly 99% at any flow rate, with the cyclohexane selectivity slightly descending from 98% to 93% with rising WHSV. After 8 h on-stream, the reaction becomes even more sensitive to changes in WHSV. The cyclohexanol selectivity rises from 2% to 36% and the cyclohexane selectivity drops from 86% to 42% between 1.8 and 3.0 h^{-1}. This indicates some kind of saturation or depletion effect which affects the ratio of feed and active sites and therefore regulates the reaction kinetically. Thus, low WHSV respective long contact time promotes consecutive

reactions of intermediates (e.g., cyclohexanol, cyclohexene) toward cyclohexane or MCP. To obtain the highest possible hydrogenation depth, a WHSV of 1.8 h^{-1} is favored.

Table 5. Effect of WHSV on phenol HDO over 10Ni10Co/HZSM-5 in the flow reactor.

TOS (h)	WHSV (h^{-1})	Conversion (%)	Selectivity (%)					
			Cyclo-hexane	Benzene	Cyclo-hexene	MCP	Cyclo-hexanol	Cyclo-hexanone
1	1.8	99.5	96.3	1.8	0.9	0.5	0.5	-
	2.2	100	95.5	1.9	2.5	-	-	-
	3.0	100	92.9	2.4	4.0	0.3	0.5	-
4	1.8	100	94.6	3.6	1.4	0.4	-	-
	2.2	100	91.9	2.6	4.8	0.3	0.5	-
	3.0	100	77.9	3.9	11.2	-	6.6	0.4
8	1.8	100	86.0	6.5	5.7	0.3	1.5	-
	2.2	100	77.9	5.2	11.2	0.3	5.5	-
	3.0	100	42.2	4.4	14.5	-	35.8	3.0

Reaction conditions: T = 250 °C, p = 60 bar, H_2: phenol molar ratio = 28, catalyst weight = 0.3, 0.4 and 0.5 g, respectively.

2.5. Evaluation of 24-Hour Hydrodeoxygenation (HDO) Runs Using 10Ni10Co/HZSM-5 or 21Ni/HZSM-5

To better understand the catalyst stability, prolonged runs over 24 h on-stream were carried out with 10Ni10Co/HZSM-5 and 21Ni/HZSM-5 at the favored conditions (T = 250 °C, p = 60 bar H_2, WHSV = 1.8 h^{-1}, 3 wt % phenol in H_2O, H_2: phenol molar ratio = 28) (Figure 8).

With 10Ni10Co/HZSM-5, phenol conversion stayed complete over 24 h on-stream, but decreased for 21Ni/HZSM-5 from 100% to 83%. Possible reasons for activity loss are the augmented deposition of carbonaceous material on the surface and the stronger losses of specific surface area, acidity (see Tables 1 and 2) and active metal by leaching (Table 6) from the monometallic catalyst. Regarding the measured extent of these changes, mostly the loss of surface area, formation of deposits and loss of active metal seem to cause the faster deactivation of 21Ni/HZSM-5. According to inductively coupled plasma-optical emission spectroscopy (ICP-OES) and atomic adsorption spectroscopy (AAS) results, the Ni content in 21Ni/HZSM-5 decreased by 6.5 wt %, whereas the Ni and Co contents in 10Ni10Co/HZSM-5 were only lowered by 1.9 wt % and 1.8 wt %, respectively. This indicates the improved hydrothermal stability of the Ni-Co alloy compared to neat Ni as active metal.

Some other changes, particularly related to the support, are very similar for both the catalysts: the Si and Al contents of the support in 21Ni/HZSM-5 were slightly reduced by 5.0 and 0.7 wt %, respectively, whereas the losses in the 10Ni10Co/HZSM-5 amounted to 4.7 and 0.9 wt %. These results are attributed to the dissolution of Si and Al in the aqueous phase [60–62]. In addition, acidities of BS and LS of both catalysts declined at nearly the same rate (see Tables 1 and 2). These effects may not contribute to the observed deactivation of the monometallic catalyst at least during the TOS studied; however, they might play a role at prolonged operation times. Significantly, some selectivity changes can be clearly seen, obviously due to some loss in acidity-suppressing deoxygenation. Figure 8 illustrates that selectivity to cyclohexanone and cyclohexanol raised from zero to 10% and 14%, respectively, within 24 h.

In addition, the nature of the metal species definitely determines the stability with regard to deep hydrogenation. The enhanced Ni particle growth in 21Ni/HZSM-5 might be one reason for declining activity. The observed changes of metal particle size and shape in the spent catalysts might influence the adsorption modes of reactants on various sites (e.g., steps and corners). In line with this, it was suggested that the metal particle sizes could be related to different pathways in phenol HDO over Ru/TiO_2 catalyst, leading to different product distribution [40]. Various active sites in Ni/SiO_2 catalyst showed different rates in hydrogenation and dehydration during phenol HDO [53,63] and this was explained by metal particle size, as dehydration was hindered on small particles due to competitive adsorption of alcohols.

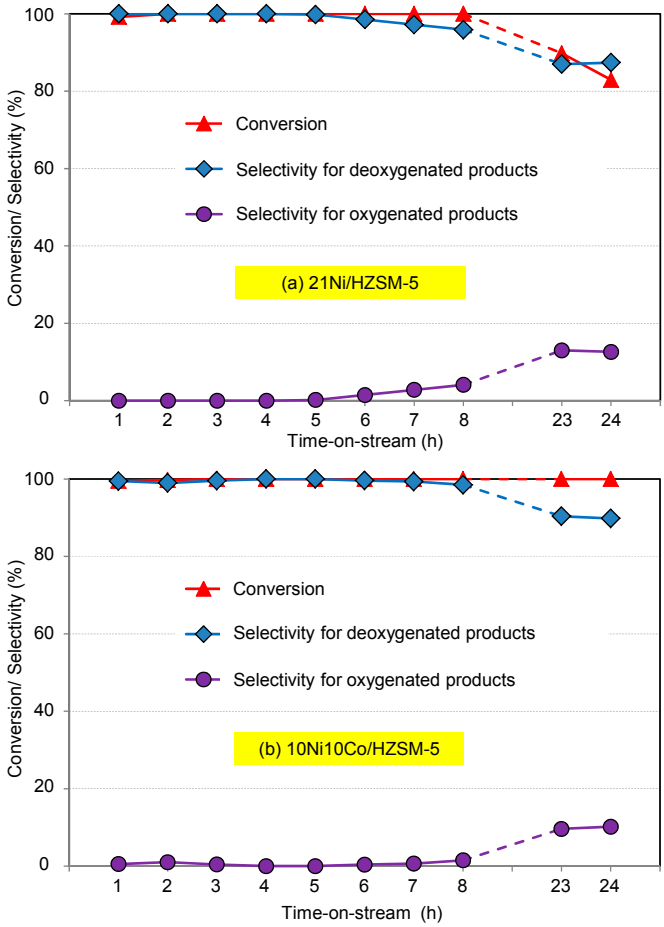

Figure 8. Phenol HDO in the continuous reactor over (**a**) 21Ni/HZSM-5 and (**b**) 10Ni10Co/HZSM-5 (T = 250 °C, p = 60 bar, WHSV = 1.8 h^{-1}, H_2:phenol molar ratio = 28).

Table 6. Loss of metal atoms in supported HZSM-5 catalysts after 24 h on-stream based on inductively coupled plasma-optical emission spectroscopy (ICP-OES) and atomic adsorption spectroscopy (AAS) results.

Catalyst	Relative Loss (wt %)			
	Ni	Co	Si	Al
10Ni10Co/HZSM-5	1.9	1.8	4.7	0.7
21Ni/HZSM-5	6.5	-	5.0	0.9

On the other side, the bimetallic catalyst forms Ni-Co alloy which stabilizes small Ni particles and is more resistant to leaching. Table 7 provides data on the product distribution with TOS. A slight decrease in selectivity toward oxygen-free hydrocarbons from 100% to 90% was noticeable with 10Ni10Co/HZSM-5 after 24 h, and 21Ni/HZSM-5 showed a decline in selectivity from 100% to 86%. However, after 24 h, the selectivity shifted from cyclohexane to unsaturated intermediates cyclohexene and benzene to a larger extent with the monometallic (28%) than with the bimetallic catalyst (22%). This increase of benzene and cyclohexene formation at the expense of cyclohexane was not properly seen in batch-wise experiments. Consequently, the highest amount of carbonaceous material was observed on 21Ni/HZSM-5, partly filling the pores and blocking some active sites, thus influencing the rates of individual reaction steps and finally the selectivity. The change in the

selectivities observed in the long-term runs in the present study is therefore attributed to the slight drop of acid sites, a loss of metal sites, and also the changes in particle sizes and shapes.

Table 7. Product distribution over HZSM-5-supported catalysts.

TOS (h)	Catalysts	Conversion (%)	Selectivity (%)					
			Cyclo-hexane	Benzene	Cyclo-hexene	MCP	Cyclo-hexanol	Cyclo-hexanone
1	21Ni	99.2	94.4	3.6	1.6	0.4	-	-
	10Ni10Co	99.5	96.3	1.8	0.9	0.5	0.5	-
4	21Ni	100	90.8	4.9	4.0	0.4	-	-
	10Ni10Co	100	94.6	3.6	1.4	0.4	-	-
8	21Ni	100	72.6	7.8	15.3	0.2	2.9	1.2
	10Ni10Co	100	86.0	6.5	5.7	0.3	1.5	-
24	21Ni	83.1	59.1	10.1	17.8	0.5	8.5	4.1
	10Ni10Co	100	68.1	10.4	11.0	0.3	7.5	2.6

Reaction conditions: T = 250 °C, p = 60 bar, WHSV = 1.8 h^{-1}, H_2:phenol molar ratio = 28.

3. Materials and Methods

3.1. Catalyst Preparation

All monometallic and bimetallic catalysts were prepared by the wet (co-)impregnation method. $Ni(NO_3)_2 \cdot 6H_2O$ (Merck) and $Co(NO_3)_2 \cdot 6H_2O$ (Fluka) were used as precursors for Ni and Co, respectively. Common zeolites HZSM-5 (PZ-2/25H, SiO_2/Al_2O_3 = 34, Zeochem AG), HBeta (PB/H, SiO_2/Al_2O_3 = 25, Zeochem AG) and NH_4Y (CBV712, SiO_2/Al_2O_3 = 12, Zeolyst) together with ZrO_2 (Saint Gobain) were used as supports. Prior to impregnation, NH_4Y was calcined (550 °C, 4 h) to get the HY form. The other supports were calcined at 450 °C for 2 h to remove physisorbed water. The calculated amount of precursor was dissolved in a known amount of deionized water and the solution was then impregnated onto supports under stirring at room temperature (RT) for 16 h. Water was removed by a rotary evaporator and the samples were ground, dried overnight and calcined (550 °C, 4 h). These samples are denoted as "fresh". The calcined catalyst was reduced in a tubular quartz reactor in pure H_2 flow (100 mL/min) with a heating rate of 10 K/min to 650 °C and kept for 4 h. These samples are denoted as "pre-reduced".

3.2. Catalyst Characterization

The metal (Ni, Co, Al) and Si contents of the samples were determined by inductively coupled plasma-optical emission spectroscopy (ICP-OES) using a 715-ES device (Varian, Inc., Palo Alto, CA, USA) and atomic adsorption spectroscopy (AAS) using an Analyst 300 apparatus (PerkinElmer, Inc., Waltham, MA, USA), respectively. The coke deposition on spent catalyst was analyzed using a Truespace CHNS analyzer (LECO Corporation, Saint Joseph, MI, USA).

Nitrogen physisorption method served for calculating the specific surface area according to the BET theory. The measurements were performed on a Micromeritics ASAP 2010 apparatus (Micromeritics GmbH, Aachen, Germany) at −196 °C. Prior to analysis, the calcined catalysts were degassed at 200 °C in vacuum for 4 h.

X-ray powder diffraction (XRD) measurements were carried out by a X'Pert Pro theta/theta diffractometer (Panalytical B.V., Almelo, Netherlands) with CuKα radiation (λ = 1.5418 Å, 40 kV, 40 mA) and an X'Celerator RTMS Detector (Panalytical B.V., Almelo, Netherlands). The samples were scanned in the 2θ range of 5°–80° and the Scherrer equation was used for crystallite size calculation.

X-ray photoelectron spectroscopy (XPS) measurements were carried out with a VG ESCALAB 220iXL instrument (Thermo Fisher Scientific, Inc., Waltham, MA, USA) with monochromatic AlKα radiation (E = 1486.6 eV). The peak areas were determined after background subtraction and fitting with Gaussian-Lorentzian curves. The amount of each component in the near-surface region can be

calculated based on these peak areas with division by the element-specific Scofield factor and the transmission function of the spectrometer.

Infrared spectroscopic measurements of adsorbed pyridine (pyr-IR) were used for acidity characterization and were carried out on a Tensor 27 spectrometer (Bruker Optik GmbH, Ettlingen, Germany) equipped with a homemade reaction cell with CaF_2 windows. The pre-reduced catalysts were pretreated in 5% H_2/He at 400 °C for 10 min. After cooling to room temperature (RT) and evacuation, the pyridine adsorption was performed until saturation. Then, the reaction cell was evacuated to remove physisorbed pyridine and finally the desorption of pyridine was followed by heating the sample in vacuum to 300 °C and recording spectra every 50 K.

Transmission electron microscopy (TEM) was employed to gain more information on metal sites, their dispersion and particle size on the catalysts. The measurements were performed at 200 kV on a JEM-ARM200F (JEOL (Germany) GmbH, Freising, Germany) which is aberration-corrected by a CESCOR (CEOS) for the scanning transmission (STEM) applications. The microscope is equipped with a JED-2300 (JEOL) energy dispersive X-ray spectrometer (EDXS) for chemical analysis. High-angle annular dark field (HAADF) combined with EDXS imaging was operated with a spot size of 0.16 nm and a 40 µm condenser aperture. For the bright field STEM images, annular bright field (BF) with beam stopper and a 3 mm BF aperture was used. The sample was ground and deposited on a holey carbon-supported Cu grid and transferred to the microscope.

3.3. HDO of Phenol in Batch Reactor

In a typical test, 0.5 g (5.3 mmol) phenol (Merck), 10 g H_2O, and 0.025 g of pre-reduced catalyst (in powder form) were loaded into an autoclave (25 mL volume; Parr Instruments, Moline, IL, USA). The reactor was flushed with Ar and then with H_2 to remove air, pressurized with H_2 to 50 bar at RT and heated to 250 °C. The start time was recorded when the reaction temperature was reached and then stirring speed was set to 650 rpm. After reaction, the autoclave was cooled to RT and the gas was analyzed by gas chromatography using a HP 5890 device (Hewlett-Packard, Inc., Palo Alto, CA, USA) online from autoclave via a transfer line. This gas chromatograph (GC) was equipped with both flame ionization detector (FID) (Poraplot Q column, 25 m × 0.53 mm × 0.20 µm) and thermal conductivity detector (TCD) (HP PLOT Molesieve column, 25 m × 0.53 mm) both using Ar as carrier gas. Liquid products (organic and aqueous phase) were analyzed by a Shimadzu GC 17A apparatus (Shimadzu Deutschland GmbH, Duisburg, Germany) with autosampler and FID (CP-FFAP column, 25 m × 0.32 mm) using He as carrier gas. Mesitylene and 1,4-dioxane were used as the internal standards for quantification of organic and aqueous phase, respectively. Pure components were used for peak identification and calibration.

Conversion and selectivity (product distribution) were calculated basing on the number of carbon moles defined as follows:

$$\text{Conversion} = \frac{\text{moles of phenol consumed}}{\text{moles of initial phenol fed}} \times 100\% \quad (1)$$

$$\text{Selectivity} = \frac{\text{moles of C atoms in each product}}{\text{total moles of C atoms in the products}} \times 100\% \quad (2)$$

Carbon balances were calculated from detected products in gas and liquid phase and reached more than 90% in this work. Missing carbon was due to deposits on the surface of catalysts, some unknown minor peaks in chromatograms and losses during work-up.

3.4. HDO of Phenol in a Continuous Fixed Bed Reactor

The setup consisted of a stainless steel tubular reactor (i.d. = 5 mm, l = 310 mm, V = 7 mL, material: SS316) that was heated by an electric heating jacket. Reactor temperature was controlled by using a thermocouple placed inside the heating jacket. In addition, a movable thermocouple was placed in a

guiding tube (1/16") inside the reactor to measure the temperature of the catalyst bed. The reactor was placed in a heating box (set to 150 °C) to avoid undesired downstream condensation.

Liquid feed (3 wt % phenol in water was kept constant in this study) was dosed with a flowrate of 0.5 mL/min by an HPLC pump (Gilson, Middleton, WI, USA). The declared space velocity (WHSV) refers to x g catalyst (x = 0.3, 0.4 and 0.5 g, respectively) and 0.9 g phenol/h metered as aqueous solution per hour. N_2 (as auxiliary gas) and H_2 were fed from commercial cylinders (Air Liquide, 99.999%) downward into the reactor. The outlet of the reactor was connected to a countercurrent water cooler. Backpressure regulation (Swagelok, Solon, OH, USA) was used to release the reaction pressure to ambient and then the gas and liquid were separated in a system of two parallel separators (switchable with a three-way valve) that was placed in iced water to avoid any vaporization and escape of products. The scheme of the continuous setup is given in Figure 9.

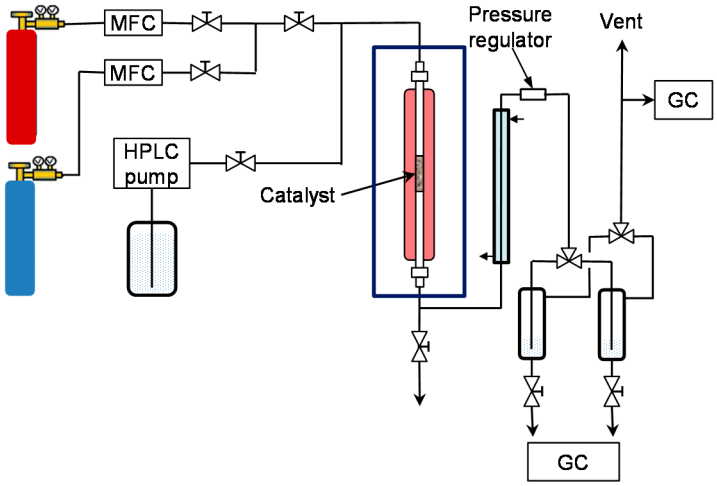

Figure 9. Schematic setup of the continuous fixed bed reactor.

The catalyst for continuous runs was shaped into pellets, then crushed to a particle size of 180–250 µm (0.3–0.5 g). The catalyst was diluted with silica (100–160 µm, Supelco) to get a volume of reaction zone of 2 mL that was placed between two silica layers and quartz wool plugs at each reactor end. Prior to each run, the externally pre-reduced catalyst was treated again at 450 °C in H_2 flow of 100 mL/min for 30 min and then cooled to RT in N_2 at 50 mL/min. Then, the feed solution was pumped to the reactor up to the desired pressure, then H_2 was fed into the reactor and finally the catalyst bed was heated to reaction temperature. The system was run at least for 2 h to achieve steady-state operation. Thus, the standard test program for each catalyst consisted of 3 h for stabilization and subsequently 8 h or more on-stream at the desired temperature. The liquid effluent was collected over 15 min in the separator in which toluene was preloaded as absorbent. The aqueous and toluene phases were analyzed by the above described GCs. Only small traces of toluene and cyclohexane (together with non-converted H_2) were found in the gas phase, thus only the liquid phase was taken into account for calculation of conversion and selectivity.

Conversion and selectivity (product distribution) were calculated from the number of carbon moles in inlet and outlet stream with the following equations:

$$\text{Conversion} = \frac{\text{moles on} - \text{stream of phenol consumed}}{\text{moles on} - \text{stream of phenol fed}} \times 100\% \quad (3)$$

$$\text{Selectivity} = \frac{\text{moles on} - \text{stream of C atoms in each product}}{\text{total moles on} - \text{stream of C atoms in the products}} \times 100\% \quad (4)$$

The carbon balances of all these experiments were >93%.

4. Conclusions

Aqueous phase hydrodeoxygenation (HDO) of phenol with Ni-Co-based catalysts in both batch and continuous flow mode reveals the best performance using HZSM-5 as support compared to HBeta, HY and ZrO_2. This is connected first to its high acid site density and strength, because such sites promote oxygen-removing steps like dehydration. The second crucial feature is the high hydrothermal stability. Therefore, the 10Ni10Co/HZSM-5 catalyst sample is the most stable catalyst and revealed the best catalytic performance. However, some deactivation with respect to particle growth, surface area decrease and acidity drop may be seen.

Ni-Co alloyed particles, as evidenced by TEM, seem to be better suited than the corresponding monometallic nickel catalysts, because Co stabilizes small Ni species, even in grown particles. The strong temperature dependence of conversion and particularly selectivity is based on two major effects: First, hydrogenation on Ni-Co metal sites starts at quite low temperatures around 200 °C, whereas the activation energy for C-O cleavage is higher and thus dehydration steps need temperatures above 225 °C. Second, at temperatures above 250 °C, undesired dehydrogenation towards benzene and isomerization come to the foreground, and chemical equilibrium rules the product distribution.

The initial catalyst screening with a batch autoclave was useful for catalyst discrimination and evaluating the effect of some reaction parameters (e.g., H_2 pressure, temperature). However, after transferring the reaction to continuous mode, some crucial features of the catalyst performance—specifically related to deactivation such as surface blocking, metal particle agglomeration, and loss of active metal and acidity—could be observed. Interestingly, some of these effects seem to affect the deoxygenation selectivity rather than the phenol conversion.

Acknowledgments: The authors gratefully acknowledge financial support by Petrovietnam and LIKAT. We want to thank U. Bentrup, M. Schneider, J. Radnik, R. Eckelt, A. Lehmann and A. Simmula (all at LIKAT) for their analytical support.

Author Contributions: T.M.H, A.M. and U.A. conceived and designed the experiments; T.M.H. performed the experiments; T.M.H., U.A., L.H.N., B.M.Q.P., D.A.N. analyzed the data; C.R.K. performed the TEM measurement; T.M.H. and U.A. wrote the paper.

Conflicts of Interest: The authors declare no conflict of interest.

References

1. BP Statistical Review of World Energy. June 2015. Available online: http://www.bp.com/en/global/corporate/about-bp/energy-economics/statistical-review-of-world-energy.html (accessed on 24 May 2015).
2. Dincer, I. Renewable energy and sustainable development: A crucial review. *Renew. Sustain. Energy Rev.* **2000**, *4*, 157–175. [CrossRef]
3. Carpenter, D.; Westover, T.L.; Czernik, S.; Jablonski, W. Biomass feedstocks for renewable fuel production: A review of the impacts of feedstock and pretreatment on the yield and product distribution of fast pyrolysis bio-oils and vapors. *Green Chem.* **2014**, *16*, 384–406. [CrossRef]
4. Melero, J.A.; Iglesias, J.; Garcia, A. Biomass as renewable feedstock in standard refinery units. Feasibility, opportunities and challenges. *Energy Environ. Sci.* **2012**, *5*, 7393–7420. [CrossRef]
5. Furimsky, E. Catalytic hydrodeoxygenation. *Appl. Catal. A* **2000**, *199*, 147–190. [CrossRef]
6. Elliott, D.C. Historical Developments in Hydroprocessing Bio-oils. *Energy Fuels* **2007**, *21*, 1792–1815. [CrossRef]
7. Laurent, E.; Delmon, B. Influence of water in the deactivation of a sulfided catalyst during hydrodeoxygenation. *J. Catal.* **1994**, *146*, 281–291. [CrossRef]
8. Romero, Y.; Richard, F.; Brunet, S. Hydrodeoxygenation of 2-ethylphenol as a model compound of bio-crude over sulfided Mo-based catalysts: Promoting effect and reaction mechanism. *Appl. Catal. B* **2010**, *98*, 213–223. [CrossRef]
9. Wildschut, J.; Mahfud, F.H.; Venderbosch, R.H.; Heeres, H.J. Hydrotreatment of Fast Pyrolysis Oil Using Heterogeneous Noble-Metal Catalysts. *Ind. Eng. Chem. Res.* **2009**, *48*, 10324–10334. [CrossRef]

10. Hong, D.-Y.; Miller, S.J.; Agrawal, P.K.; Jones, C.W. Hydrodeoxygenation and coupling of aqueous phenolics over bifunctional zeolite-supported metal catalysts. *Chem. Commun.* **2010**, *46*, 1038–1040. [CrossRef] [PubMed]
11. Runnebaum, R.; Nimmanwudipong, T.; Block, D.; Gates, B. Catalytic Conversion of Anisole: Evidence of Oxygen Removalin Reactions with Hydrogen. *Catal. Lett.* **2011**, *141*, 817–820. [CrossRef]
12. Sitthisa, S.; Pham, T.; Prasomsri, T.; Sooknoi, T.; Mallinson, R.G.; Resasco, D.E. Conversion of furfural and 2-methylpentanal on Pd/SiO_2 and $Pd–Cu/SiO_2$ catalysts. *J. Catal.* **2011**, *280*, 17–27. [CrossRef]
13. Sitthisa, S.; Resasco, D. Hydrodeoxygenation of Furfural over Supported Metal Catalysts: A Comparative Study of Cu, Pd and Ni. *Catal. Lett.* **2011**, *141*, 784–791. [CrossRef]
14. Zhu, X.; Lobban, L.L.; Mallinson, R.G.; Resasco, D.E. Bifunctional transalkylation and hydrodeoxygenation of anisole over a Pt/HBeta catalyst. *J. Catal.* **2011**, *281*, 21–29. [CrossRef]
15. Ausavasukhi, A.; Huang, Y.; To, A.T.; Sooknoi, T.; Resasco, D.E. Hydrodeoxygenation of *m*-cresol over gallium-modified beta zeolite catalysts. *J. Catal.* **2012**, *290*, 90–100. [CrossRef]
16. Ohta, H.; Kobayashi, H.; Hara, K.; Fukuoka, A. Hydrodeoxygenation of phenols as lignin models under acid-free conditions with carbon-supported platinum catalysts. *Chem. Commun.* **2011**, *47*, 12209–12211. [CrossRef] [PubMed]
17. Li, N.; Huber, G.W. Aqueous-phase hydrodeoxygenation of sorbitol: Identification of the reaction pathway. *J. Catal.* **2010**, *270*, 48–59. [CrossRef]
18. Lee, C.R.; Yoon, J.S.; Suh, Y.-W.; Choi, J.-W.; Ha, J.-M.; Suh, D.J.; Park, Y.-K. Catalytic roles of metals and supports on hydrodeoxygenation of lignin monomer guaiacol. *Catal. Commun.* **2012**, *17*, 54–58. [CrossRef]
19. Zhao, C.; He, J.; Lemonidou, A.A.; Li, X.; Lercher, J.A. Aqueous-phase hydrodeoxygenation of bio-derived phenols to cycloalkanes. *J. Catal.* **2011**, *280*, 8–16. [CrossRef]
20. Zhao, C.; Kou, Y.; Lemonidou, A.A.; Li, X.; Lercher, J.A. Highly Selective Catalytic Conversion of Phenolic Bio-Oil to Alkanes. *Angew. Chem. Int. Ed.* **2009**, *48*, 3987–3990. [CrossRef] [PubMed]
21. Zhang, X.; Wang, T.; Ma, L.; Zhang, Q.; Jiang, T. Hydrotreatment of bio-oil over Ni-based catalyst. *Bioresour. Technol.* **2013**, *127*, 306–311. [CrossRef] [PubMed]
22. Mortensen, P.M.; Grunwaldt, J.-D.; Jensen, P.A.; Jensen, A.D. Screening of Catalysts for Hydrodeoxygenation of Phenol as a Model Compound for Bio-oil. *ACS Catal.* **2013**, *3*, 1774–1785. [CrossRef]
23. Zhao, C.; Kasakov, S.; He, J.; Lercher, J.A. Comparison of kinetics, activity and stability of Ni/HZSM-5 and Ni/Al_2O_3-HZSM-5 for phenol hydrodeoxygenation. *J. Catal.* **2012**, *296*, 12–23. [CrossRef]
24. Sitthisa, S.; Sooknoi, T.; Ma, Y.; Balbuena, P.B.; Resasco, D.E. Kinetics and mechanism of hydrogenation of furfural on Cu/SiO_2 catalysts. *J. Catal.* **2011**, *277*, 1–13. [CrossRef]
25. Olcese, R.N.; Bettahar, M.; Petitjean, D.; Malaman, B.; Giovanella, F.; Dufour, A. Gas-phase hydrodeoxygenation of guaiacol over Fe/SiO_2 catalyst. *Appl. Catal. B* **2012**, *115–116*, 63–73. [CrossRef]
26. Deutsch, K.L.; Shanks, B.H. Hydrodeoxygenation of lignin model compounds over a copper chromite catalyst. *Appl. Catal. A* **2012**, *447–448*, 144–150. [CrossRef]
27. Alonso, D.M.; Wettstein, S.G.; Dumesic, J.A. Catalytic conversion of biomass to biofuels. *Green Chem.* **2010**, *12*, 1493–1513. [CrossRef]
28. Ardiyanti, A.R.; Khromova, S.A.; Venderbosch, R.H.; Yakovlev, V.A.; Heeres, H.J. Catalytic hydrotreatment of fast-pyrolysis oil using non-sulfided bimetallic Ni-Cu catalysts on a -Al_2O_3 support. *Appl. Catal. B* **2012**, *117–118*, 105–117. [CrossRef]
29. Do, P.T.M.; Foster, A.J.; Chen, J.; Lobo, R.F. Bimetallic effects in the hydrodeoxygenation of meta-cresol on γ-Al_2O_3 supported Pt–Ni and Pt–Co catalysts. *Green Chem.* **2012**, *14*, 1388–1397. [CrossRef]
30. Sun, J.; Karim, A.M.; Zhang, H.; Kovarik, L.; Li, X.S.; Hensley, A.J.; McEwen, J.-S.; Wang, Y. Carbon-supported bimetallic Pd–Fe catalysts for vapor-phase hydrodeoxygenation of guaiacol. *J. Catal.* **2013**, *306*, 47–57. [CrossRef]
31. Hong, Y.; Zhang, H.; Sun, J.; Ayman, K.M.; Hensley, A.J.R.; Gu, M.; Engelhard, M.H.; McEwen, J.-S.; Wang, Y. Synergistic Catalysis between Pd and Fe in Gas Phase Hydrodeoxygenation of m-Cresol. *ACS Catal.* **2014**, *4*, 3335–3345. [CrossRef]
32. Leng, S.; Wang, X.; He, X.; Liu, L.; Liu, Y.; Zhong, X.; Zhuang, G.; Wang, J.G. $NiFe/\gamma$-Al_2O_3: A universal catalyst for the hydrodeoxygenation of bio-oil and its model compounds. *Catal. Commun.* **2013**, *41*, 34–37. [CrossRef]

33. Nie, L.; de Souza, P.M.; Noronha, F.B.; An, W.; Sooknoi, T.; Resasco, D.E. Selective conversion of m-cresol to toluene over bimetallic Ni–Fe catalysts. *J. Mol. Catal. A: Chem.* **2014**, *388–389*, 47–55. [CrossRef]
34. Bykova, M.V.; Ermakov, D.Y.; Kaichev, V.V.; Bulavchenko, O.A.; Saraev, A.A.; Lebedev, M.Y.; Yakovlev, V.A. Ni-based sol–gel catalysts as promising systems for crude bio-oil upgrading: Guaiacol hydrodeoxygenation study. *Appl. Catal. B* **2012**, *113–114*, 296–307. [CrossRef]
35. Choudhary, T.V.; Phillips, C.B. Renewable fuels via catalytic hydrodeoxygenation. *Appl. Catal. A* **2011**, *397*, 1–12. [CrossRef]
36. Bu, Q.; Lei, H.; Zacher, A.H.; Wang, L.; Ren, S.; Liang, J.; Wei, Y.; Liu, Y.; Tang, J.; Zhang, Q.; et al. A review of catalytic hydrodeoxygenation of lignin-derived phenols from biomass pyrolysis. *Bioresour. Technol.* **2012**, *124*, 470–477. [CrossRef] [PubMed]
37. Wang, H.; Male, J.; Wang, Y. Recent Advances in Hydrotreating of Pyrolysis Bio-Oil and Its Oxygen-Containing Model Compounds. *ACS Catal.* **2013**, *3*, 1047–1070. [CrossRef]
38. Saidi, M.; Samimi, F.; Karimipourfard, D.; Nimmanwudipong, T.; Gates, B.C.; Rahimpour, M.R. Upgrading of lignin-derived bio-oils by catalytic hydrodeoxygenation. *Energy Environ. Sci.* **2014**, *7*, 103–129. [CrossRef]
39. Massoth, F.E.; Politzer, P.; Concha, M.C.; Murray, J.S.; Jakowski, J.; Simons, J. Catalytic Hydrodeoxygenation of Methyl-Substituted Phenols: Correlations of Kinetic Parameters with Molecular Properties. *J. Phys. Chem. B* **2006**, *110*, 14283–14291. [CrossRef] [PubMed]
40. Newman, C.; Zhou, X.; Goundie, B.; Ghampson, I.T.; Pollock, R.A.; Ross, Z.; Wheeler, M.C.; Meulenberg, R.W.; Austin, R.N.; Frederick, B.G. Effects of support identity and metal dispersion in supported ruthenium hydrodeoxygenation catalysts. *Appl. Catal. A* **2014**, *477*, 64–74. [CrossRef]
41. Zhao, C.; Lercher, J.A. Selective Hydrodeoxygenation of Lignin-Derived Phenolic Monomers and Dimers to Cycloalkanes on Pd/C and HZSM-5 Catalysts. *ChemCatChem* **2012**, *4*, 64–68. [CrossRef]
42. De Souza, P.M.; Rabelo-Neto, R.C.; Borges, L.E.P.; Jacobs, G.; Davis, B.H.; Sooknoi, T.; Resasco, D.E.; Noronha, F.B. Role of Keto Intermediates in the Hydrodeoxygenation of Phenol over Pd on Oxophilic Supports. *ACS Catal.* **2015**, *5*, 1318–1329. [CrossRef]
43. Mortensen, P.M.; Gardini, D.; de Carvalho, H.W.P.; Damsgaard, C.D.; Grunwaldt, J.-D.; Jensen, P.A.; Wagner, J.B.; Jensen, A.D. Stability and resistance of nickel catalysts for hydrodeoxygenation: Carbon deposition and effects of sulfur, potassium, and chlorine in the feed. *Catal. Sci. Technol.* **2014**, *4*, 3672–3686. [CrossRef]
44. Echeandia, S.; Pawelec, B.; Barrio, V.L.; Arias, P.L.; Cambra, J.F.; Loricera, C.V.; Fierro, J.L.G. Enhancement of phenol hydrodeoxygenation over Pd catalysts supported on mixed HY zeolite and Al_2O_3. An approach to O-removal from bio-oils. *Fuel* **2014**, *117*, 1061–1073. [CrossRef]
45. Le, T.A.; Ly, H.V.; Kim, J.; Kim, S.-S.; Choi, J.H.; Woo, H.-C.; Othman, M.R. Hydrodeoxygenation of 2-furyl methyl ketone as a model compound in bio-oil from pyrolysis of Saccharina Japonica Alga in fixed-bed reactor. *Chem. Eng. J.* **2014**, *250*, 157–163. [CrossRef]
46. Dickinson, J.G.; Savage, P.E. Development of NiCu Catalysts for Aqueous-Phase Hydrodeoxygenation. *ACS Catal.* **2014**, *4*, 2605–2615. [CrossRef]
47. Yoon, Y.; Rousseau, R.; Weber, R.S.; Mei, D.; Lercher, J.A. First-Principles Study of Phenol Hydrogenation on Pt and Ni Catalysts in Aqueous Phase. *J. Am. Chem. Soc.* **2014**, *136*, 10287–10298. [CrossRef] [PubMed]
48. Huynh, T.M.; Armbruster, U.; Pohl, M.-M.; Schneider, M.; Radnik, J.; Hoang, D.-L.; Phan, B.M. Q.; Nguyen, D.A.; Martin, A. Hydrodeoxygenation of Phenol as a Model Compound for Bio-oil on Non-noble Bimetallic Nickel-based Catalysts. *ChemCatChem* **2014**, *6*, 1940–1951. [CrossRef]
49. Huynh, T.M.; Armbruster, U.; Phan, B.M.Q.; Nguyen, D.A.; Martin, A. The influence of cobalt in bimetallic Ni-Co catalyst supported on H-Beta for phenol hydrodeoxygenation. *Chim. Oggi* **2014**, *32*, 40–44.
50. Huynh, T.M.; Armbruster, U.; Nguyen, L.H.; Nguyen, D.A.; Martin, A. Hydrodeoxygenation of Bio-Oil on Bimetallic Catalysts: From Model Compound to Real Feed. *JSBS* **2015**, *5*, 151–160. [CrossRef]
51. Huynh, T.M.; Armbruster, U.; Atia, H.; Bentrup, U.; Phan, B.M.Q.; Eckel, R.; Nguyen, L.H.; Nguyen, D.A.; Martin, A. Upgrading of bio-oil and subsequent co-processing under FCC conditions for fuel production. *React. Chem. Eng.* **2016**, *1*, 239–251. [CrossRef]
52. Emeis, C.A. Determination of Integrated Molar Extinction Coefficients for Infrared Absorption Bands of Pyridine Adsorbed on Solid Acid Catalysts. *J. Catal.* **1993**, *141*, 347–354. [CrossRef]
53. Mortensen, P.M.; Grunwaldt, J.-D.; Jensen, P.A.; Jensen, A.D. Influence on nickel particle size on the hydrodeoxygenation of phenol over Ni/SiO_2. *Catal. Today* **2016**, *259*, 277–284. [CrossRef]

54. Kruse, A.; Dinjus, E. Hot compressed water as reaction medium and reactant. Properties and synthesis reactions. *J. Supercrit. Fluids* **2007**, *39*, 362–380. [CrossRef]
55. Kruse, A.; Dinjus, E. Hot compressed water as reaction medium and reactant: 2. Degradation reactions. *J. Supercrit. Fluids* **2007**, *41*, 361–379. [CrossRef]
56. Ravenelle, R.M.; Schüβler, F.; D'Amico, A.; Danilina, N.; van Bokhoven, J.A.; Lercher, J.A.; Jones, C.W.; Sievers, C. Stability of Zeolites in Hot Liquid Water. *J. Phys. Chem. C* **2010**, *114*, 19582–19595. [CrossRef]
57. Jentys, A.; Lercher, J.A. Techniques of zeolite characterization. In *Studies in Surface Science and Catalysis*; van Bekkum, H., Flanigen, E.M., Jacobs, P.A., Jansen, J.C., Eds.; Elsevier B.V.: Amsterdam, The Netherlands, 2001; Volume 137, pp. 345–386.
58. Gandarias, I.; Barrio, V.L.; Requies, J.; Arias, P.L.; Cambra, J.F.; Güemez, M.B. From biomass to fuels: Hydrotreating ofoxygenated compounds. *Int. J. Hydrog. Energy* **2008**, *33*, 3485–3488. [CrossRef]
59. Germain, J.E. *Catalytic Conversion of Hydrocarbons*; Academic Press: London, UK, 1969.
60. Van Donk, S.; Janssen, A.H.; Bitter, J.H.; de Jong, K.P. Generation, Characterization, and Impact of Mesopores in Zeolite Catalysts. *Catal. Rev.* **2003**, *45*, 297–319. [CrossRef]
61. Groen, J.C.; Peffer, L.A.A.; Moulijn, J.A.; Pérez-Ramírez, J. Mechanism of Hierarchical Porosity Development in MFI Zeolites by Desilication: The Role of Aluminium as a Pore-Directing Agent. *Chem. Eur. J.* **2005**, *11*, 4983–4994. [CrossRef] [PubMed]
62. Abelló, S.; Bonilla, A.; Pérez-Ramírez, J. Mesoporous ZSM-5 zeolite catalysts prepared by desilication with organic hydroxides and comparison with NaOH leaching. *Appl. Catal. A* **2009**, *364*, 191–198. [CrossRef]
63. Mortensen, P.M. Catalytic Conversion of Bio-oil to Fuel for Transportation. Ph.D. Thesis, Technical University of Denmark, Lyngby, Denmark, 2013.